Dynamics and field-induced order in the layered spin *S* = 1/2 dimer system (C₅H₆N₂F)₂CuCl₄

D. Blosser, M. Horvatić, R. Bewley, S. Gvasaliya
and A. Zheludev

Dynamics and field-induced order in the layered spin $S = 1/2$ dimer system $(C_5H_6N_2F)_2CuCl_4$

D. Blosser,[1,*] M. Horvatić,[2] R. Bewley,[3] S. Gvasaliya,[1] and A. Zheludev[1,†]

[1]*Laboratory for Solid State Physics, ETH Zürich, 8093 Zürich, Switzerland*

[2]*Laboratoire National des Champs Magnétiques Intenses, LNCMI-CNRS (UPR3228), EMFL, UGA, UPS, and INSA, Boîte Postale 166, 38042 Grenoble Cedex 9, France*

[3]*ISIS Facility, Rutherford Appleton Laboratory, Chilton, Didcot, Oxon OX11 0QX, United Kingdom*

The quasi-two-dimensional Heisenberg spin $S = 1/2$ dimer system bis(2-amino-5-fluoro-pyridinium) tetra-chlorocuprate(II) is studied by means of inelastic neutron scattering, calorimetry, and nuclear magnetic resonance (NMR) experiments. In the absence of an applied magnetic field we find dispersive triplet excitations with a spin gap of $\Delta = 1.112(15)$ meV and a bandwidth of 0.715(15) meV within the layers and 0.116(15) meV between the layers, respectively. In an applied magnetic field of $\mu_0 H_c \approx 8.5$ T the spin gap is closed and we find a field-induced antiferromagnetically ordered phase.

I. INTRODUCTION

Organometallic transition-metal halogen salts have provided a great variety of interesting magnetic model systems. In these compounds magnetic transition-metal ions are linked by halogen mediated superexchange bridges. Due to the large size and magnetic inertness of the organic cations, exceptionally clean quasi-low-dimensional magnetic systems have been realized in such compounds. Furthermore, the magnetic exchange energy is typically on the order of 1 meV, i.e., ~ 10 K or ~ 10 T in units of temperature or magnetic field, respectively, allowing experimental studies of these compounds in their full temperature and magnetic field phase diagram.

Very prominent quasi-one-dimensional organometallic model compounds include the prototypical strong-rung and strong-leg spin ladders $(C_5H_{12}N)_2CuBr_4$ (BPCB) [1–6] and $(C_7H_{10}N)_2CuBr_4$ (DIMPY) [7–13], respectively, or the ferromagnetic rung spin ladder $(CH_3)_2CHNH_3CuCl_3$ (IPA-CuCl$_3$) [14–16].

Finding similar model compounds of quasi-two-dimensional spin systems would be very exciting for the experimental study of such systems and significant effort has been focused on this quest. One notable example of a quasi-two-dimensional spin system among the organometallic transition-metal halogen salts is $(C_4H_{12}N_2)Cu_2Cl_6$ (PHCC) [17–20] which features a rather complicated and partially frustrated quasi-two-dimensional network of spin dimers. Another whole family of compounds that has attracted attention as candidates for quasi-two-dimensional magnetic model compounds is $(py)_2CuHa_4$, where py stands for a pyridine-based cation and Ha for a halogen [21–27].

Here, we report on a detailed experimental investigation of the compound bis(2-amino-5-fluoropyridinium) tetra-chlorocuprate(II), $(C_5H_6N_2F)_2CuCl_4$ or $(5FAP)_2CuCl_4$ for

short [25]. In this compound, the magnetic Cu^{2+} ions are linked by Cu-Cl$\cdots$Cl-Cu superexchange bridges into a layered network of dimers [28]. By means of inelastic neutron scattering experiments we precisely quantify the magnetic exchange interactions and we find non-negligible interactions in all three crystallographic directions. In an applied magnetic field, we find a field-induced magnetically ordered phase (BEC of magnons) which we characterize by measurements of specific heat and nuclear magnetic resonance.

II. EXPERIMENT

A. Crystal structure and magnetic exchange pathways

$(5FAP)_2CuCl_4$ crystallizes in a monoclinic $P2_1/c$ structure with lattice constants $a = 6.926(7)$ Å, $b = 21.73(2)$ Å, $c = 10.911(10)$ Å, and $\beta = 100.19°$ [25]. There are four Cu^{2+} ions per unit cell. These are arranged in buckled $[CuCl_4]^{2-}$ anion layers and $[C_5H_6N_2F]^+$ cation layers stacked along the crystallographic a direction as shown in Fig. 1 [29].

The dominant magnetic exchange interaction J shown in Fig. 1 as blue solid lines connects pairs of Cu^{2+} ions to form spin dimers. The weaker interaction J_1 links the dimers in the (b, c) planes. These layers are topologically equivalent to a square lattice of weakly coupled dimers, or to a honeycomb lattice as sketched in Fig. 1(b). The stacking of the layers in the crystal structure is shown in Fig. 1(c). Possible magnetic interaction pathways between the layers J_2, J_3 are indicated in Fig. 1(d) [30].

B. Synthesis and crystal growth

For all our measurements we require single-crystal samples. Furthermore, in neutron scattering experiments hydrogen leads to very strong incoherent scattering (background in our experiments) necessitating the use of deuterated 2-amino-5-fluoropyridine (d5FAP). This is obtained from protonated 5FAP by catalytic H/D substitution [31,32] as follows: 4 g

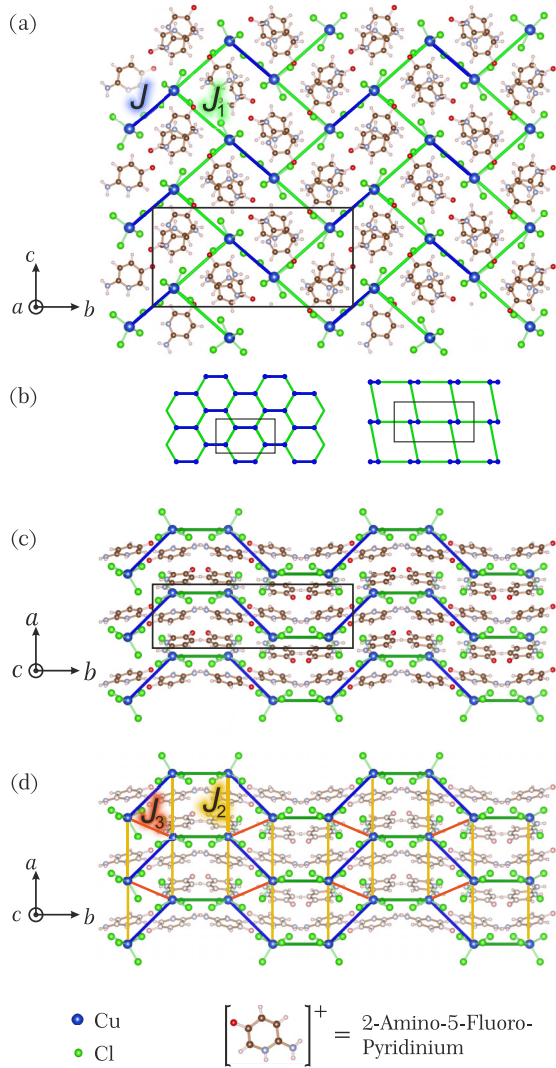*dblosser@phys.ethz.ch

†zhelud@ethz.ch; http://www.neutron.ethz.ch/

FIG. 1. (a) Crystal structure of $(5FAP)_2CuCl_4$ projected along the crystallographic a direction. The blue lines show the dominant magnetic interaction J forming spin dimers. These are coupled in the b, c planes (J_1, green lines) creating 2D layers of coupled dimers. These are topologically equivalent to a honeycomb lattice or to a square lattice of dimers as sketched in (b). (c), (d) Crystal structure as projected along c illustrating the buckled layers. Possible interlayer interactions are marked by orange and red lines.

of 5FAP is slurried in 62.3 ml of D_2O in a polytetrafluoroethylene (PTFE) lined 125-ml pressure vessel with 200 mg of Pd/C (10 wt.%) catalyst. The pressure vessel is closed under Ar atmosphere with 10 ml of H_2 gas. For the substitution reaction to occur, the vessel is kept at $180\,°C$ for 72 h while continuously stirring. Finally, after filtering off the catalyst and drying the product, $\sim 70\%$ deuterated 2-amino-5-fluoropyridine is obtained as confirmed by mass spectroscopy.

Single crystals are grown by slowly cooling a saturated solution: d5FAP (21 mmol) and $CuCl_2$ (10.5 mmol) are dissolved in 15 ml D_2O and 5.4 ml of DCl in D_2O (35 wt.%) [25]. The obtained solution is evaporated to obtain approximately 10 ml of saturated solution at $15\,°C$. Small seed crystals are hanged into the solution on a thin PTFE thread. Slowly cooling the saturated solution from 15 to $2\,°C$ at a rate of

0.5 K/day, large green high-quality single crystals of $m \approx 0.4$ g are obtained.

C. Experimental methods

All our experiments are performed on $\sim 70\%$ deuterated single-crystal samples with the applied magnetic field aligned with the crystallographic b direction [33].

1. Inelastic neutron scattering

For the neutron scattering experiments six crystals (approximately 70% deuterated) were wrapped in a thin PTFE film [34], coaligned to within $1.5°$ and fixed on an aluminum sample holder. The neutron scattering experiments where performed at the LET time-of-flight spectrometer [35] at the ISIS facility, U.K. The sample was mounted on a dilution refrigerator in a 9-T cryomagnet with the crystallographic b direction parallel to the magnetic field, i.e., perpendicular to the scattering plane. Making use of repetition rate multiplication, data were simultaneously collected using $E_i = 2.1, 3.5,$ and 6.9 meV incident energy neutrons. The data [36] have been analyzed using the HORACE software package [37].

2. Specific heat

Specific heat was measured on a $m = 1.15(8)$ mg single crystal using a Quantum Design physical properties measurement system (PPMS) equipped with a ^{3}He-^{4}He dilution refrigerator insert.

3. Nuclear magnetic resonance

^{19}F (nuclear spin $I = 1/2$) NMR experiments were performed on a single crystal of dimension $\sim 3.6 \times 1.2 \times 0.9$ mm with an rf coil precisely fitting the sample dimension. This assembly is mounted inside the mixing chamber of a ^{3}He-^{4}He dilution refrigerator ensuring good thermalization. The external magnetic field is applied parallel to the crystallographic b direction. The nuclear relaxation rate $1/T_1$ is obtained from the spin-echo intensity $M(t)$ measured as a function of time t after a saturating pulse by fitting the exponential function $M(t) = M_{eq} - M_0 \exp\{-(t/T_1)\}$ to the data where M_{eq} is the intensity in thermal equilibrium. These data were measured at the spectral center or at the upper peak when the spectrum is split within the ordered phase. At several points inside the ordered phase, we verified that the thus obtained T_1 is identical for both of the split peaks.

III. RESULTS AND DISCUSSION

A. Inelastic neutron scattering

Neutron scattering intensities were measured at $T = 100$ mK in zero field as a function of energy and wave-vector transfer to obtain a large four-dimensional data set $\mathcal{I}(\mathbf{Q}, \omega)$. Representative cuts through these data are shown in Fig. 2. The false-color plots show scattering intensity versus energy and momentum transfer, where the data has been integrated in slices of ± 0.1 reciprocal lattice units (r.l.u.) along the reciprocal space directions not shown in the plots.

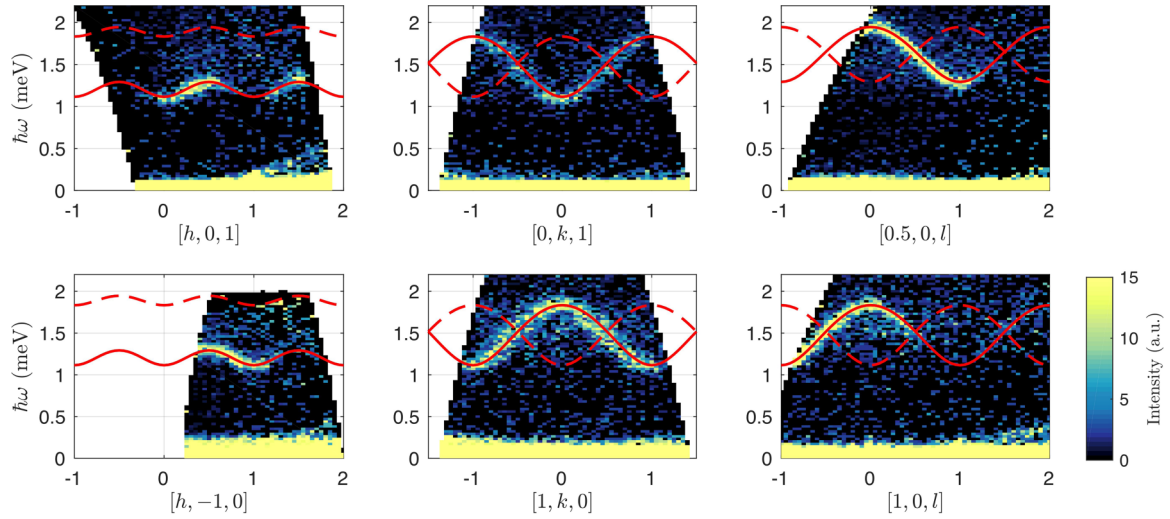We find resolution-limited dispersive triplet excitations with a spin gap of $\Delta = 1.112(15)$ meV. They show a sizable

FIG. 2. Representative false-color slices through the four-dimensional inelastic neutron scattering data set measured in $(5FAP)_2CuCl_4$ at $T = 100$ mK in zero magnetic field showing the dispersion of magnetic triplet excitations. The solid and dashed lines correspond to the calculated triplet dispersion branches as described in the text.

dispersion in the k, l directions (i.e., within the dimer planes) with a bandwidth of $\Gamma_{k,l} = 0.715(15)$ meV. The interlayer dispersion along h is significantly smaller with a bandwidth $\Gamma_h = 0.116(15)$ meV.

To determine the relevant exchange parameters we extend the procedure described in Ref. [28] to also include the possible interlayer interactions. We start by considering a lattice of two isolated dimers per unit cell with an antiferromagnetic exchange interaction J. The weaker exchange interactions J_1, J_2, J_3 between the dimers we now treat within the random phase approximation (RPA) [28,38]. For the triplet dispersion we thus find

$$(\hbar\omega_{\mathbf{q}}^{\pm})^2 = J^2 \pm JR(T)[J_1(\cos\pi(k+l) + \cos\pi(k-l)) \pm (J_2 - 2J_3)\cos(2\pi h)], \quad (1)$$

with $R(T) = \frac{1-e^{-J/(k_BT)}}{1+3e^{-J/(k_BT)}}$ denoting the difference in population of the singlet and triplet states of an isolated dimer. As there are two dimers per unit cell we naturally find two excitation branches. However, in almost all of reciprocal space accessed in our experiments only one excitation branch carries all the intensity. Fits of this dispersion to the neutron scattering data are shown in Fig. 2 as solid and dashed lines. The fitted estimates for the exchange parameters are

$$J = 1.586(8) \text{ meV},$$
$$J_1 = 0.333(7) \text{ meV},$$
$$(J_2 - 2J_3) = -0.139(8) \text{ meV}. \quad (2)$$

At the RPA level, the dispersion only contains the sum $(J_2 - 2J_3)$ of the possible exchange interactions between the planes and we cannot determine J_2 and J_3 independently. However, the relevant magnetic exchange interactions between the Cu^{2+} ions are mediated by Cu-Cl$\cdots$Cl-Cu superexchange pathways leading to antiferromagnetic exchange ($J > 0$). Ferromagnetic interactions ($J < 0$) seem unlikely in this setting [39,40]. Since for $(J_2 - 2J_3)$ a negative value is found, we expect that the interplane interactions are predominantly due to

J_3. Moreover, the relevant Cl$\cdots$Cl separation for J_2 is larger than for J_3, again pointing to J_3 as the dominant interlayer coupling. Assuming $J_2 = 0$, we find a ratio $J_3/J_1 = 0.21$ of the interlayer versus in-plane coupling strength, quantifying the quasi-two-dimensionality of this compound.

In an applied magnetic field, the threefold degeneracy of the triplet modes is lifted and the two dispersion branches are Zeeman-split into six bands. This we clearly see in neutron scattering data obtained at $\mu_0 H = 5$ and 6.8 T. From these data sets we extract the band extrema as shown in Fig. 3(a). From the field dependence of the Zeeman shift we can directly determine the g-factor in this geometry as $g_b = 2.13(2)$. Extrapolating the low-energy triplet band minimum we expect the spin gap to close at $\mu_0 H \approx 9$ T. Indeed, in an applied magnetic field slightly below this value, at low temperatures we find a phase transition to a magnetically ordered state
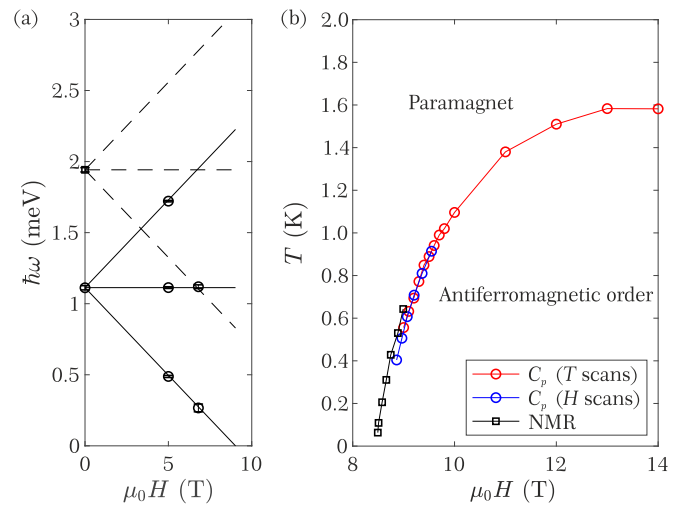

FIG. 3. (a) Band extrema of the Zeeman-split triplet modes as a function of magnetic field. (b) Phase boundary of the field-induced long-range ordered antiferromagnetic phase as measured by specific heat and nuclear magnetic resonance.
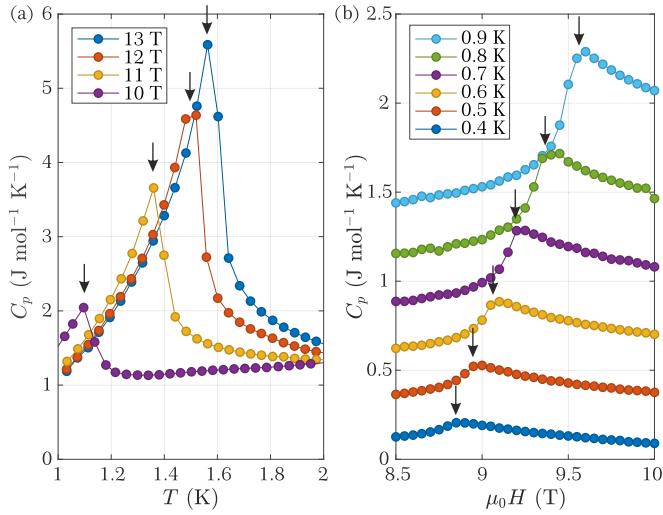
FIG. 4. Representative measurements of specific heat vs (a) temperature and (b) magnetic field. Peaks mark the onset of long-range antiferromagnetic order.

as revealed by measurements of specific heat and nuclear magnetic resonance.

B. Specific heat

Specific heat was measured in a wide range of temperatures and magnetic fields up to 14 T. Representative data versus temperature and magnetic field, respectively, are shown in Fig. 4. At high magnetic fields, we find a very strong and very sharp peak in specific heat versus temperatures [Fig. 4(a)]. Towards lower temperatures and closer to the critical field H_c, the magnitude of the peak decreases and it broadens. Data traces of specific heat versus magnetic field measured at lower temperatures [Fig. 4(b)] also reveal a maximum that decreases and broadens towards lower temperatures. Below 0.4 K pinpointing the phase boundary becomes impossible. The reason for this decrease and broadening of the peaks remains unclear.

The phase boundary extracted from these data is plotted in Fig. 3(b). It has a maximum near 13.5 T where it occurs at a temperature of $T_N = 1.58$ K. Towards zero temperature the phase boundary extrapolates to a value slightly below 9 T, consistent with the field where the spin gap closes as estimated from the inelastic neutron scattering data. Assuming the phase boundary to show a roughly symmetric "dome" shape between the lower critical field H_c and the field of saturation H_{sat}, we expect an upper critical field of $\mu_0 H_{sat} \approx$ 18–19 T, in line with the saturation field estimated from high-field magnetization measurements [25].

C. Nuclear magnetic resonance

To investigate the nature of the phase transition and of the field-induced long-range ordered phase we turn to NMR measurements of the ^{19}F nuclear spin ($I = 1/2$). Measurements of both the NMR spectrum as well as the nuclear spin relaxation rate have been performed at various magnetic fields and temperatures. In the $(5FAP)_2CuCl_4$ crystal structure there are two inequivalent F sites at low-symmetry positions. Nonetheless, the NMR lines from the two sites apparently overlap and therefore could not be distinguished.

For $\mu_0 H = 9$ T, representative NMR spectra are depicted in Fig. 5(a). While we observe a single sharp resonance line at elevated temperatures, upon cooling this line slightly broadens and splits, confirming a transition to an antiferromagnetic state.

Analyzing the evolution of the spectrum in more detail, in Figs. 5(b) and 5(c) we show the apparent line splitting taken as the distance between the peaks, whenever two distinct maxima are visible. This simple measure will slightly underestimate the antiferromagnetic order parameter in the regime where the splitting is of similar size as the width of the individual lines. However, we note that the lines do not only split, but also the line shape changes across the transition. For this reason, fitting a double-peak function to the measured spectra to more accurately extract the line splitting has not proven useful.
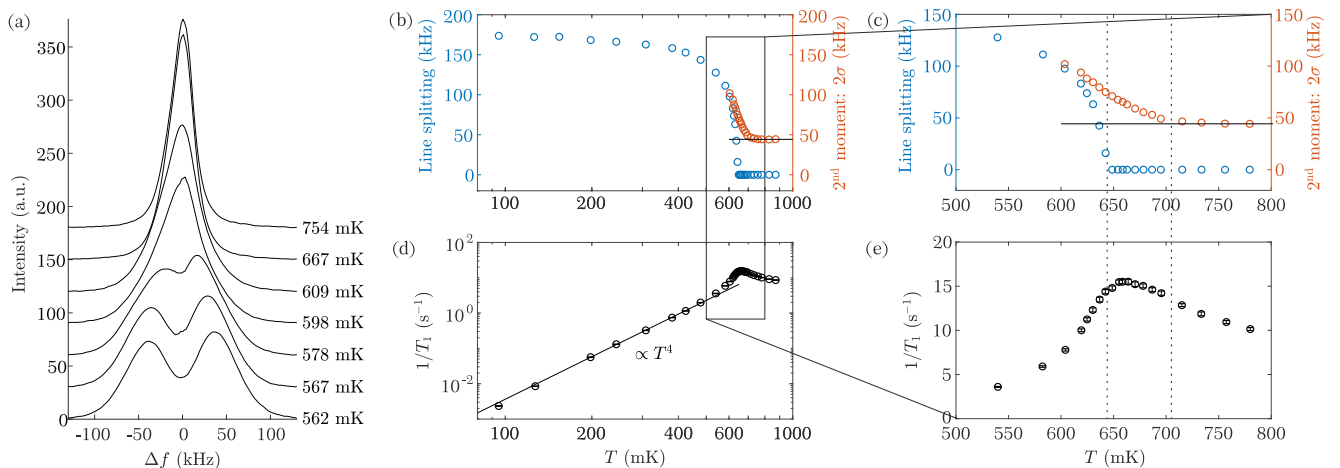

FIG. 5. NMR data measured at $\mu_0 H = 9$ T. (a) Evolution of the ^{19}F NMR spectrum upon entering the ordered phase. The splitting of the resonance indicates antiferromagnetic long-range order. (b), (c) Temperature evolution of the line splitting and (d), (e) the nuclear spin relaxation rate $1/T_1$.
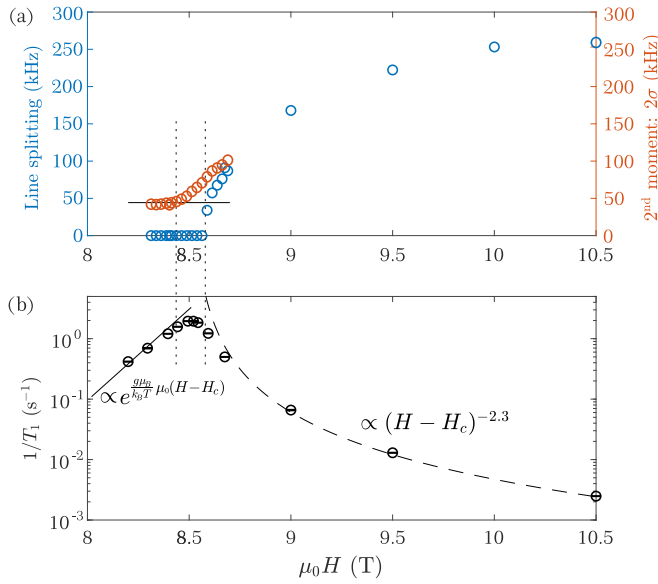
FIG. 6. (a) NMR line broadening and splitting and (b) $1/T_1$ relaxation rate vs magnetic field at $T = 206$ mK.

A different and well-defined measure of the observed spectra is the second moment shown as 2σ in Figs. 5(b) and 5(c) [41]. Regardless of the line shape, for strongly split peaks, 2σ exactly corresponds to the line splitting. We observe that already at temperatures roughly 50 mK above the appearance of two distinct peaks, the line starts to broaden and its second moment increases. The onset of this line broadening directly reflects the onset of slow fluctuations with a frequency that is lower than the ^{19}F nuclear spin Larmor frequency of $f_0 \sim 360$ MHz at the field of 9 T.

Measurements of the nuclear spin relaxation rate $1/T_1$ at 9 T are plotted in Figs. 5(d) and 5(e). At low temperatures, well inside the ordered phase, we observe a $1/T_1 \propto T^4$ power-law dependence over almost one decade in temperature. The high value of the power-law exponent is only slightly smaller than what is usually observed in BEC phases of quantum antiferromagnets (5.0–5.5) [42,43], reflecting a high-order relaxation process [44]. In the vicinity of the transition, we find a rounded peak with a maximum at slightly higher temperatures than the appearance of the apparent line splitting.

Similar data measured at a constant temperature of $T = 206$ mK versus magnetic field are shown in Fig. 6. We again observe a broadening of the NMR line (characterized by the second moment) followed by a splitting into two peaks. Again, the phase transition is accompanied by a maximum

in $1/T_1$ at $\mu_0 H = 8.51$ T, slightly before the line splitting becomes apparent. Taking this value as the critical field H_c, at lower fields we expect an exponential reduction of the relaxation rate $1/T_1 \propto e^{\frac{g\mu_B}{k_B T}\mu_0(H-H_c)}$, indicative of the opening of a spin gap. (Here, using the previously determined value of $g = 2.13$, the only unknown parameter is an overall prefactor.) We only have very few data points below the critical field but they roughly seem to follow the expected trend. Inside the ordered phase, phenomenologically, the data follow a power-law behavior $1/T_1 \propto (H - H_c)^{-\kappa}$ with an exponent $\kappa \approx 2.3$.

We performed spectral NMR measurements at various temperatures and magnetic fields. From these data we have extracted the phase boundary as the point where two distinct maxima become visible in the spectrum. These points are shown in the phase diagram of Fig. 3(b). At low temperatures the phase boundary becomes very steep and seems consistent with a $T_N \propto (H - H_c)^{2/3}$ behavior as has been observed in fully three-dimensional systems [45]. However, from the present data it is impossible to reliably extract a critical exponent. We observe a slight mismatch between the points obtained from NMR measurements and the position of the phase boundary extracted from specific heat data. Since for these measurements two different samples were used, we suspect this small difference to be due to slightly different transition fields in the two samples, or a slightly different alignment of the crystals with respect to the applied magnetic field in the two experiments.

IV. CONCLUSION

The layered spin dimer compound $(5\text{FAP})_2\text{CuCl}_4$ has been studied in detail. We find a singlet ground state and dispersive triplet excitations separated by a spin gap of $\Delta = 1.112(15)$ meV. The triplon dispersion shows a bandwidth of $\Lambda_{k,l} = 0.715(15)$ meV within the dimer planes and $\Lambda_h = 0.116(15)$ meV between the layers.

Measurements of specific heat and nuclear magnetic resonance reveal a field-induced antiferromagnetically ordered phase beyond $\mu_0 H_c \approx 8.5$ T extending up to 1.58 K at 13.5 T.

[1] B. R. Patyal, B. L. Scott, and R. D. Willett, Phys. Rev. B **41**, 1657 (1990).

[2] C. Rüegg, K. Kiefer, B. Thielemann, D. F. McMorrow, V. Zapf, B. Normand, M. B. Zvonarev, P. Bouillot, C. Kollath, T. Giamarchi, S. Capponi, D. Poilblanc, D. Biner, and K. W. Krämer, Phys. Rev. Lett. **101**, 247202 (2008).

[3] A. T. Savici, G. E. Granroth, C. L. Broholm, D. M. Pajerowski, C. M. Brown, D. R. Talham, M. W. Meisel, K. P. Schmidt, G. S. Uhrig, and S. E. Nagler, Phys. Rev. B **80**, 094411 (2009).

[4] B. Thielemann, C. Rüegg, H. M. Rønnow, A. M. Läuchli, J.-S. Caux, B. Normand, D. Biner, K. W. Krämer, H.-U. Güdel, J. Stahn, K. Habicht, K. Kiefer, M. Boehm, D. F. McMorrow, and J. Mesot, Phys. Rev. Lett. **102**, 107204 (2009).

[5] M. Klanjšek, H. Mayaffre, C. Berthier, M. Horvatić, B. Chiari, O. Piovesana, P. Bouillot, C. Kollath, E. Orignac, R. Citro, and T. Giamarchi, Phys. Rev. Lett. **101**, 137207 (2008).

[6] D. Blosser, V. K. Bhartiya, D. J. Voneshen, and A. Zheludev, Phys. Rev. Lett. **121**, 247201 (2018).

[7] A. Shapiro, C. P. Landee, M. M. Turnbull, J. Jornet, M. Deumal, J. J. Novoa, M. A. Robb, and W. Lewis, J. Am. Chem. Soc. **129**, 952 (2007).

[8] T. Hong, Y. H. Kim, C. Hotta, Y. Takano, G. Tremelling, M. M. Turnbull, C. P. Landee, H.-J. Kang, N. B. Christensen, K. Lefmann, K. P. Schmidt, G. S. Uhrig, and C. Broholm, Phys. Rev. Lett. **105**, 137207 (2010).

[9] D. Schmidiger, P. Bouillot, S. Muhlbauer, S. Gvasaliya, C. Kollath, T. Giamarchi, and A. Zheludev, Phys. Rev. Lett. **108**, 167201 (2012).

[10] D. Schmidiger, P. Bouillot, T. Guidi, R. Bewley, C. Kollath, T. Giamarchi, and A. Zheludev, Phys. Rev. Lett. **111**, 107202 (2013).

[11] M. Jeong, H. Mayaffre, C. Berthier, D. Schmidiger, A. Zheludev, and M. Horvatić, Phys. Rev. Lett. **111**, 106404 (2013).

[12] K. Y. Povarov, D. Schmidiger, N. Reynolds, R. Bewley, and A. Zheludev, Phys. Rev. B **91**, 020406(R) (2015).

[13] M. Jeong, D. Schmidiger, H. Mayaffre, M. Klanjšek, C. Berthier, W. Knafo, G. Ballon, B. Vignolle, S. Krämer, A. Zheludev, and M. Horvatić, Phys. Rev. Lett. **117**, 106402 (2016).

[14] H. Manaka, I. Yamada, and K. Yamaguchi, J. Phys. Soc. Jpn. **66**, 564 (1997).

[15] T. Masuda, A. Zheludev, H. Manaka, L.-P. Regnault, J.-H. Chung, and Y. Qiu, Phys. Rev. Lett. **96**, 047210 (2006).

[16] A. Zheludev, V. O. Garlea, T. Masuda, H. Manaka, L.-P. Regnault, E. Ressouche, B. Grenier, J.-H. Chung, Y. Qiu, K. Habicht, K. Kiefer, and M. Boehm, Phys. Rev. B **76**, 054450 (2007).

[17] L. P. Battaglia, A. B. Corradi, U. Geiser, R. D. Willett, A. Motori, F. Sandrolini, L. Antolini, T. Manfredini, L. Menabue, and G. C. Pellacani, J. Chem. Soc., Dalton Trans. 265 (1988).

[18] M. B. Stone, I. Zaliznyak, D. H. Reich, and C. Broholm, Phys. Rev. B **64**, 144405 (2001).

[19] G. Perren, J. S. Möller, D. Hüvonen, A. A. Podlesnyak, and A. Zheludev, Phys. Rev. B **92**, 054413 (2015).

[20] S. Bettler, G. Simutis, G. Perren, D. Blosser, S. Gvasaliya, and A. Zheludev, Phys. Rev. B **96**, 174431 (2017).

[21] H. Place and R. D. Willett, Acta Crystallogr., Sect. C **43**, 1050 (1987).

[22] F. M. Woodward, A. S. Albrecht, C. M. Wynn, C. P. Landee, and M. M. Turnbull, Phys. Rev. B **65**, 144412 (2002).

[23] P. R. Hammar, D. C. Dender, D. H. Reich, A. S. Albrecht, and C. P. Landee, J. Appl. Phys. **81**, 4615 (2002).

[24] F. C. Coomer, V. Bondah-Jagalu, K. J. Grant, A. Harrison, G. J. McIntyre, H. M. Rønnow, R. Feyerherm, T. Wand, M. Meißner, D. Visser, and D. F. McMorrow, Phys. Rev. B **75**, 094424 (2007).

[25] L. Li, M. M. Turnbull, C. P. Landee, J. Jornet, M. Deumal, J. J. Novoa, and J. L. Wikaira, Inorg. Chem. **46**, 11254 (2007).

[26] A. J. Gale, C. P. Landee, M. M. Turnbull, and J. L. Wikaira, Polyhedron **52**, 986 (2013).

[27] C. A. Krasinski, B. L. Solomon, F. F. Awwadi, C. P. Landee, M. M. Turnbull, and J. L. Wikaira, J. Coord. Chem. **70**, 914 (2017).

[28] T. Hong, S. N. Gvasaliya, S. Herringer, M. M. Turnbull, C. P. Landee, L.-P. Regnault, M. Boehm, and A. Zheludev, Phys. Rev. B **83**, 052401 (2011).

[29] The crystal structure plots shown in Fig. 1 are based on renderings generated by the VESTA software package [46].

[30] In Ref. [28], for the interlayer coupling, erroneously only J_2 had been considered which was argued to be exponentially weaker than the in-plane interactions as it has a much larger Cl-Cl separation (5.07 Å) than the in-plane exchange pathways (3.66 and 4.07 Å). However, also considering J_3 for which there are two possible exchange pathways with a Cl-Cl separation of 4.24 and 4.45 Å, we certainly cannot expect the interlayer interactions to be negligible.

[31] H. Esaki, N. Ito, S. Sakai, T. Maegawa, Y. Monguchi, and H. Sajiki, Tetrahedron **62**, 10954 (2006).

[32] J. Atzrodt, V. Derdau, T. Fey, and J. Zimmermann, Angew. Chem., Int. Ed. **46**, 7744 (2007).

[33] Additional heat capacity data were measured on a fully protonated crystal and the results were virtually identical with the data obtained on ∼70% deuterated samples. Also, the lattice constants of the crystal do not change measurably upon deuteration. For this reason we do not expect any significant difference between protonated and deuterated samples. Similarly, we do not expect the partial deuteration to cause any "disorder" in regard to the sample's magnetic properties.

[34] It was found that $(5FAP)_2CuCl_4$ chemically reacts with aluminum on a timescale of a few weeks.

[35] R. Bewley, J. Taylor, and S. Bennington, Nucl. Instrum. Methods Phys. Res., Sect. A **637**, 128 (2011).

[36] D. Blosser and A. Zheludev, Field induced $z = 2$ quantum criticality in a quasi-2D quantum magnet, STFC ISIS Neutron and Muon Source, https://doi.org/10.5286/ISIS.E.98093410 (2018).

[37] R. Ewings, A. Buts, M. Le, J. van Duijn, I. Bustinduy, and T. Perring, Nucl. Instrum. Methods Phys. Res., Sect. A **834**, 132 (2016).

[38] J. Jensen and A. Mackintosh, *Rare Earth Magnetism: Structures and Excitations*, International Series of Monographs on Physics (Clarendon, Oxford, UK, 1991).

[39] P. Straatman, R. Block, and L. Jansen, Phys. Rev. B **29**, 1415 (1984).

[40] C. P. Landee and M. M. Turnbull, Eur. J. Inorg. Chem. **2013**, 2266 (2013).

[41] The second moment σ of a peak-shaped function $f(x)$ about its mean μ is defined as $\sigma^2 = \frac{1}{A} \int_{-\infty}^{\infty} (x - \mu)^2 f(x) dx$, where $\mu = \frac{1}{A} \int_{-\infty}^{\infty} x f(x) dx$ and $A = \int_{-\infty}^{\infty} f(x) dx$. The second moment provides a measure for the variance of a function. If there is a single peak, σ measures its width. For example, for a single Gaussian peak $g(x) = \frac{1}{c\sqrt{2\pi}} e^{-\frac{1}{2}(x/c)^2}$ we find $\sigma = c$. On the other hand, for two strongly separated peaks, σ measures the distance between the peaks. For the case of two Gaussians $g(x + L) + g(x - L)$ the second moment is $\sigma = \sqrt{L^2 + c^2}$, which reduces to $\sigma \approx L$ in the limit $L \gg c$. For the data analysis at hand, the second moment is thus a convenient and model-independent measure with a transparent interpretation both in the limit where we observe a single peak as well as in the limit where two strongly separated peaks are observed.

[42] H. Mayaffre, M. Horvatić, C. Berthier, M.-H. Julien, P. Ségransan, L. Lévy, and O. Piovesana, Phys. Rev. Lett. **85**, 4795 (2000).

[43] M. Jeong, H. Mayaffre, C. Berthier, D. Schmidiger, A. Zheludev, and M. Horvatić, Phys. Rev. Lett. **118**, 167206 (2017).

[44] D. Beeman and P. Pincus, Phys. Rev. **166**, 359 (1968).

[45] V. Zapf, M. Jaime, and C. D. Batista, Rev. Mod. Phys. **86**, 563 (2014).

[46] K. Momma and F. Izumi, J. Appl. Crystallogr. **44**, 1272 (2011).